J. theor. Biol. (1996) **178,** 275–294

Phyllotaxis as a Dynamical Self Organizing Process Part II: The Spontaneous Formation of a Periodicity and the Coexistence of Spiral and Whorled Patterns

S. Douady and Y. Couder

Laboratoire de Physique Statistique, 24 *rue Lhomond*, 75231 *Paris Cedex* 05, *France*

(*Received on* 12 *January* 1995, *Accepted in revised form on* 15 *August* 1995)

The conditions for the appearance of a new primordium put forward by Snow & Snow (1952) are shown to form the rules of a dynamical iterative system more general than that based on Hofmeister's hypotheses (1868). This system is simple, generic and compatible with several of the ideas about the possible nature of the interaction between primordia. By numerical simulation, it is demonstrated that this system is sufficient to spontaneously generate time periodic regimes in which the successive elements are organized either in Fibonacci spiral or in whorled modes of growth. We show that the dynamical system generally selects the pattern with the densest packing. The effect of the geometrical shape of the apex and of the primorida on the stability of the opposite decussate phyllotaxy is pointed out.

1. Introduction

In the first part of this work (Douady & Couder, 1996*a*) we demonstrated experimentally and numerically that the formation of the spiral phyllotactic patterns could be obtained by self organization in a simple iterative system working on the principles proposed by Hofmeister (1868). This system is controlled by only one parameter: Richards' plastochrone ratio (1951), which results from the velocity of the growth, the size of the apex and the period of formation of a new primordium. The periodicity is supposed to be imposed on the system by some internal or external factor.

These dynamical regimes, however, in which only one primordium forms at a time, can only give rise to the distichous and spiral modes of growth. There is no realistic way within this model to consider the whorled and multijugate modes of organization. In these arrangements several primordia appear simultaneously, forming successive nodes along the stem. They are characterized by the number n of primordia formed at each period ($n \geqslant 2$) and their relative positions. In whorled patterns the n primordia of a given node are evenly disposed around the stem at angles $\varphi = 2\pi/n$ from each other and they are in directions bisecting the angles formed by the elements of the previous node. The divergence φ' between a primordium of a node and its nearest neighbour of the next node is thus $\varphi' = \pi/n$. This divergence φ' can also be smaller than π/n; a spiral organization is then observed which can be analysed as resulting from the existence of n generative spirals. These modes are usually called the multijugate or n-jugate modes (Bravais & Bravais, 1837). Among the whorled modes, the most common is the simplest: the decussate phyllotaxy in which two elements form at each period so that $\varphi = \pi$ and $\varphi' = \pi/2$. When decussate plants undergo transitions where φ' becomes smaller than $\pi/2$, they give rise to bijugate spirals. The most common case of multijugate organization is observed in, for example, the *Dipsacus* family, which presents decussate or bijugate leaves and bijugate inflorescences. In Part I the spiral patterns were labelled (i, j) by the numbers of their parastichies in the two directions. similarly, the whorled modes with n elements at a node will be noted (n, n) or $n(1, 1)$, and the multijugate patterns (ni, nj) or $n(i, j)$.

Evidence of a close relationship between the simple spiral and the whorled modes of growth was first

given by Dutrochet (1834). Weisse (1894) found that, in several species with whorled phyllotaxis, the adventitious buds had spiral structures. From this observation he was the first to suggest that the phyllotactic mode of a stem is not fixed but depends on the initial symmetry. The transition from whorled to spiral modes of organization is observed in many plants when they develop from vegetative growth to flowering [e.g. *Epilobium hirsutum*, see Meicenheimer (1982)]. The reverse type of transition from spiral to whorl is also commonly observed during flowering. As pointed out by Schoute (1913), however, understanding floral morphology is difficult because the growth of the floral bud generally lasts only a short time: in other terms it corresponds to a rapid transient. Schoute suggested that a necessary step towards the investigation of the floral morphology would be to understand the relationship between the spiral and whorled types of organization in more steady regimes of growth; for instance in vegetative regions, or in those inflorescences where steady regimes exist.

Many works, such as those of Schoute (1922, 1925, 1936, 1938), were devoted precisely to the coexistence of spiral and whorled organizations. The transition between a whorled type of phyllotaxy and a spiral one can result from botanical experiments of the type initiated by Snow & Snow (1935). They showed that, by breaking the symmetry of an apex with a diagonal cut, a usually decussate plant (*Epilobium hirsutum*) could form spiral patterns. Revisiting the drawing of Snow & Snow, Richards (1951) showed that the formation of these spiral modes was obtained even though the plastochrone ratio was unchanged. This experiment was a demonstration of the fact that both the whorled modes and the spiral ones could result from the same dynamics with differences in the initial conditions only. It led Snow & Snow (1952) to seek a set of dynamical hypotheses that could give rise to both types of growth. They suggested a modification of the dynamical rules introduced by Hofmeister. In this new set they remove the imposed periodicity of the process and assume that a new primordium simply forms at the periphery of the apex where and when there is enough space for its formation. As discussed in Part (I), their argument involving the size of an available space is a dynamical description and is compatible with several of the hypotheses (repulsion or inhibition) about the actual mode of interaction of the primordia. Inspired by their work we will examine the regimes resulting from dynamical hypotheses in which the third and fourth rules of the initial set (Douady & Couder, 1996*a*) have been changed.

This last model is still oversimplified, however, in view of the actual morphology of the apices. In order to get a more adequate simulation of botanical reality we also took into account the fact that the apices are not planar but convex, and that the primordia can be elongated. Analysing successive slices of various apices, Williams (1975) was able to obtain complete reconstructions of their three-dimensional shape. Excellent images of apices were also obtained by scanning electron microscopy (e.g. Meicenheimer, 1979). More recently this technique, applied to moulds of a single apex taken at successive times, even permitted the direct observation of the time evolution of its shape (Hernandez *et al*., 1991; Green *et al*., 1991). All these observations show many apices to be roughly in the shape of a paraboloid. Dynamically, the important zone is the periphery of the apical meristem, a region which can be approximated by the cone tangent to the apex at this level [Fig. 1(a)]. This approximation had already been used by van Iterson (1907) and Richards (1951). If the primordium is a protrusion with a circular base on the cone, it will appear as being azimuthally elongated once projected in a plane perpendicular to the axis [Fig. 1(b)]. The

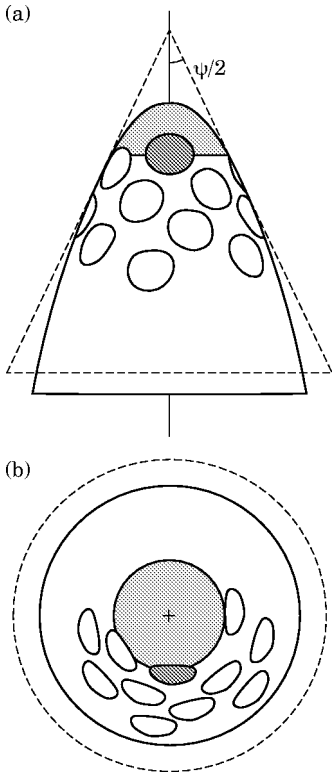

FIG. 1. (a) Scheme showing the apex and the cone tangent to it in the region of formation of the primordia (dashed lines). The cone is characterized by its angle $\Psi/2$. (b) The projection in the transverse plane. The folioid shape of the elements results from their projection. The drawings correspond to the case where the sizes of the primordia do not change as they move away from the apex.

shape of this projection was called "folioid" by Van Iterson (1907). In some plants the shape of the base of the primordia is intrinsically elongated on the paraboloid surface of the apex; this elongation is increased by the projection on a horizontal plane. We take these two effects into account simultaneously by considering elongated primordia in a plane surface. We will characterize this elongation by a parameter N to be defined below. We will not try to separate in the value of N the effect of the apex shape from that of an intrinsic elongation of the primordia. In the following, $1/N$, for simplicity, will be called the conicity.

With folioid shaped elements it is necessary to revisit the definition of the parastichies. For the circular disks on a plane used in Part I, the parastichies could be defined in two ways. They were the spirals passing by the points of contact of each element with its neighbours. They were also the spirals found by linking the centre of each element to the centre of its nearest neighbours. The same parastichies were obtained by the two methods and the angle of intersection of the main parastichies of opposite directions was always found to be the closest to 90°. With folioid shaped elements the contact parastichies are no longer the same as the nearest neighbour parastichies. Both definitions are used in the literature, depending on the author. While the contact parastichies are usually chosen by most botanists, some theorists prefer the nearest neighbour spirals. We will see that, in the plane, the dynamically important spirals which govern the selection of the pattern are the contact parastichies. This is related to the fact that the contact parastichies of the folioids in the plane correspond to parastichies which are both contact and nearest neighbour spirals on the initial conical surface.

Altogether, using the hypothesis of Snow & Snow and taking the conicity into account we reach a second set of hypotheses:

—The stem apex is axisymmetric.
—The apex is in the shape of a paraboloid and the primordia can have an azimuthally elongated shape.
—The primordia are formed at the periphery of the apical meristem and, because of the growth, they move away with a radial velocity $V(r)$.
—A new primordium appears when and where a large enough space has been formed at the periphery of the apex.
—Outside a region of radius R_0, there is no further reorganization leading to changes in the angular positions of the primordia.

Unlike the first set of hypotheses (Douady & Couder, 1996a), the plastochrone here is not an imposed parameter. The arrangements that will appear are now controlled by another parameter: the space needed for a primordium to form.

We will simulate these rules in a plane. Using folioid shaped primordia, we take into account the fact that the dynamically important regions can be approximated by a cone and a possible intrinsic dorsiventrality of the primordia. As in Part I, the exact geometry is not of crucial importance for the set of possible arrangements. We will show, however, that the particular value of the conicity can affect the selection of one arrangement with respect to another. This is particularly important for the competition between the decussate mode and the spiral arrangement (2,3). Some preliminary results of this simulation were given in Couder & Douady (1993).

2. The Simulation

It was not possible to use our experimental system with ferrofluid drops (Douady & Couder, 1996a) to satisfy the new set of hypotheses, so we had to rely on numerical simulations only. As stated above, they are performed in a plane radial configuration, the locus of appearance of elements being a circle C of radius R_0 (chosen as unit length $R_0 = 1$) centred at the origin. If a conical apex is to be represented, a change in the coordinates, or equivalently in the shape of the primordia, is used as described below. The elements are particles which move radially away from the circle with a velocity $V(r)$. As in Part I, the whole organization of the system derives from the choice of the position of formation of a new particle on the circle, which depends on the space left available by the previous particles. To simulate this occupation of space, each particle generates a repulsive energy $E(d)$ where d is the distance to this particle. The position of formation of a new particle will result from the total repulsion of the previous ones.

2.1. ENERGY THRESHOLD

The essential difference with the simulations presented in Part I lies in the criterion for the formation of incipient elements. We now leave free the time of appearance of a new primordium, but add the condition that it can only appear when the minimum energy becomes smaller than a chosen threshold, E_s. In practice this means that we now compute continuously in time (i.e. numerically with a

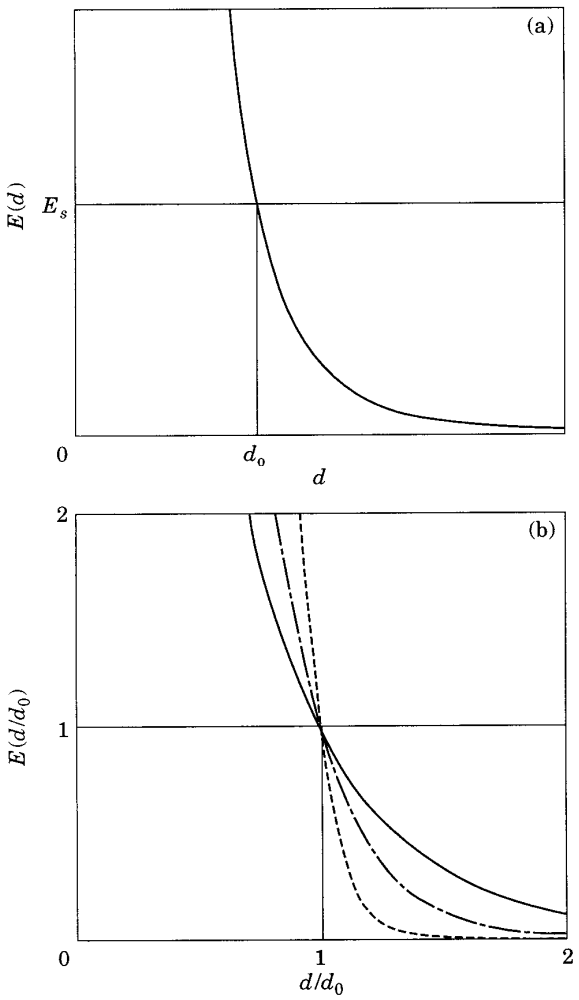

FIG. 2. (a) A potential curve $E(d)$ showing the relation of the chosen threshold E_s with the resulting size of the primordium d_0. (b) The normalized $E(d/d_0)$ dependence given by relation (1) for three values of the stiffness $\alpha=1$ (plain line), $\alpha=2$ (interrupted line) and $\alpha=4$ (dotted line).

short time step) the value of the energy in all points of the circle C. This energy, resulting from the repulsion of all the previously deposited particles, decreases as they move away. A new element is added at the point of minimum energy only at the time when the value of the potential at this minimum becomes smaller than E_s.

Let us first consider [Fig. 2(a)] a given energy law $E(d)$. We note that the chosen value of the threshold E_s corresponds to a length scale d_0 for which $E(d_0)=E_s$. The repulsive potential of each primordium thus creates a circular region of radius d_0 where the centre of a new element cannot be placed. So the minimum possible distance between the centres of two elements is d_0 and $d_0/2$ is the "radius" of a primordium. As $E(d)$ is chosen to be a monotonically decreasing function of d, it is strictly equivalent to fix the value of E_s or that of d_0. This shows that our hypotheses represent those of Snow & Snow: at the point where the incipient element forms, it is equivalent to say that the potential becomes smaller than E_s or that an available space of radius $d_0/2$ is forming.

We used several types of energy laws. The important characteristic of these potentials is what we will call the stiffness, which corresponds to the spatial spreading of the interaction. For a very stiff potential, only the first neighbours are important, while for a weak stiffness the influence of the second neighbours is not negligible.

We mostly used the interaction law:

$$E(d)=\frac{-1+\left(\tanh\alpha\dfrac{d}{d_0}\right)^{-1}}{-1+(\tanh\alpha)^{-1}} \tag{1}$$

Where tanh stands for the hyperbolic tangent. Similar results can also be obtained with the simpler power law:

$$E(d)=\frac{1}{\left(\dfrac{d}{d_0}\right)^{p}} \tag{2}$$

Both these laws are normalized with the control parameter of the system: the primordium size d_0, so that the threshold potential $E_s=E(d_0)$ is always $E_s=1$ for $d=d_0$. The stiffness of the interaction is determined by α for relation (1) and by the exponent p for relation (2).

In first approximation the results obtained with all possible repulsive laws are of the same type. As we will see, however, there are several competing modes for the organization of the particles and we found that their relative stability depended on the stiffness of the interaction. Similar results were obtained with relation (1) or (2) provided that their parameters were such that the stiffness was the same in the vicinity of $d/d_0=1$. In this region the energy profiles [Fig. 2(b)] given by relation (1) for $\alpha=1$, 2, 4 and 8 are similar to those obtained with relation (2) for $p=-3$, -5, -9, and -17 respectively. We note that for large values of α or p the interaction becomes so stiff that it becomes similar to the repulsion caused by hard disks.

In this system all the primordia have the same repulsive law, so that their size d_0 does not change as they move away from the apex. In a few simulations we explored the situations in which the size of the primordia grow larger or smaller with distance $r(t)$ to

the center. For this purpose we replaced d_0 in equations (1) and (2) by a variable size $d_p(r)$ such as:

$$d_p = d_0 \frac{r}{R_0} \tag{3}$$

where the size of the primordium is d_0 at the periphery of the central circle and grows with r for $r > R_0$. The results of such simulations are qualitatively similar to those obtained with d_0 constant. For simplicity we will mainly limit ourselves (except in Section 4.5) to elements of constant size.

The parameter that controls the state of the system is geometrical. In the planar configuration it can be defined as the ratio of the diameter of a primordium at its formation over the radius of the apex:

$$\Gamma = d_0/R_0 \tag{4}$$

In the case where the shape of the primordium is not circular, a more refined definition will be given (see the chapter below). We will call this parameter van Iterson's parameter as he used a similar one, $b = d_0/2\pi R_0$, in his geometrical analysis of the phyllotaxic pilings.

This parameter Γ has a simple geometrical meaning: it is directly related to the angle ω under which a primordium at its formation is seen from the apex center (Fig. 3). Indeed, we have for circular primordia (and $\Gamma < 2$):

$$\Gamma = 2 \sin(\omega/2) \tag{5}$$

Or, in reverse, $\omega = 2 \sin^{-1}(\Gamma/2)$. For small values of ω the sinus can be assimilated to the angle so that Γ is an approximation of ω (in radian).

2.2. THE GEOMETRY OF THE APEX

In his complete investigation of the geometrical properties of the phyllotactic arrangements, van Iterson (1907) had considered the tiling of plane, conical and cylindrical surfaces with disks. He showed the equivalence of the tiling of a cone with a tiling of the projection onto the cone's plane base. Similarly, Richards (1951) has shown how his plastochrone ratio should be modified to take conicity into account. We will use the same possibility. The interaction between the primordia occurs on a surface that we model as a cone. We assume that the interaction takes place on the surface only (i.e. is two dimensional). These interactions can be simulated in a plane by a projection of the initial surface in the plane perpendicular to the axis (Fig. 1). On the surface of the cone, constant values of the repulsive potential of a particle are circles "wrapped" around the cone. Once projected onto the plane, the equipotential circles take an azimuthally elongated folioid shape [Fig. 1(b)]. This shape is very similar to that of the cut of the primordia when observed on transverse cross sections of the apex. We can note that it is this asymmetrical shape of the folioid that will give rise to the dorsiventrality of the leaves.

In the following, all the calculations are carried out in the plane of projection for which we use polar coordinates. Considering a cone with an angle $\Psi/2$ [Fig. 1(a)] and paved with circular primordia we will characterize the shape of the folioids by $N = \sin(\Psi/2)$, the parameter that was used by van Iterson (1907). In order to obtain the interaction between two particles $E(d)$ we only need to compute the distance d between the two points on the conical surface. A point on the cone has for coordinates $(r\,\theta, z)$ with $z = -r \cos(\Psi/2)$. Thus, the height z can be omitted and the point represented in the planar projection of

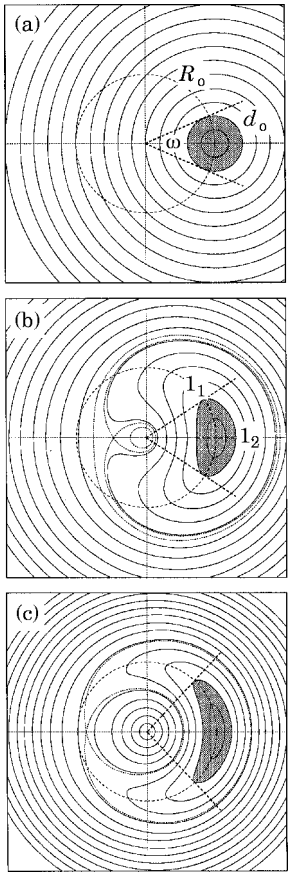

FIG. 3. The isopotential lines around a particle corresponding to three values of the conicity: (a) $1/N = 1$. The apex has a radius R_0. The shaded region corresponds to the hard core of the particle of diameter d_0. The figure also shows the angle ω sustaining the primordium at its formation. (b) $1/N = 2$, and (c) $1/N = 4$. The primordium has now the shape of a folioid of orthoradial size l_1 and radial size l_2. As above ω is the sustaining angle, note that in our choice of definition of d_0, the area covered by an element, is roughly independent of the conicity.

the cone by the point of polar coordinates (r, θ). For reasons explained in the Appendix, the true Euclidian distance on the cone between two points $P_0(r_0, \theta_0)$ and $P_1(r_1, \theta_1)$ will not be used, we replace it by a slightly modified relation:

$$d(P_0, P_1) = \sqrt{\left[\frac{r_0 - r_1^2}{N} + 2N\, r_0 r_1 (1 - \cos(\theta_0 - \theta_1)\right]} \tag{6}$$

In the following simulations we will use values of the conicity ranging from $1/N = 1$, the plane "isotropic" situation, to $1/N = 6$, which corresponds to very elongated shapes. Figure 3 shows the aspect of the isopotential lines around one single particle in three of these cases. With the definition of distances given by eqn (6) the radial size [see Fig. 1(b)] of the primordium is $l_2 = d_0 N^{1/2}$, while its orthoradial size is approximately $l_1 = d_0/N^{1/2}$. With this definition the surface of the primordium is nearly the same as in the planar case: $S \sim \pi d_0^2/4 \sim \pi l_1 l_2/4$. As in a real projection N is the ratio l_2/l_1.

The introduction of the conicity makes necessary a more general definition of the control parameter. In our preliminary work (Couder & Douady, 1993) we had chosen to take into account the average size of the primordium and thus used $\Gamma_A = d_0/R_0 = (l_1.l_2)^{1/2}/R_0$. With this parameter the threshold values Γ_A for the different modes were found to depend strongly upon the conicity. It is a common remark of the botanists (since the works of Snow & Snow, 1933) that the relevant parameter for the mode of organization is the orthoradial size of a primordium at its formation. For this reason we now choose the parameter Γ to be:

$$\Gamma = \frac{l_1}{R_0} = \frac{d_0}{N^{1/2} R_0} \tag{7}$$

In our simulation, we work with a fixed conicity N, we choose an average size d_0 of the primordia to be used in the energy computation [eqns (1) and (2)], so that the imposed Γ can be deduced from relation (7). The relation (5) can still be used as an approximation to obtain the sustaining angle ω of the primordia from Γ. The exact relation, however, which is given in the Appendix [eqn (A.3)], is more complex because of the choice of relation (6) for the computation of the distances. To give an intuitive meaning to the threshold values, our results are also given in terms of the corresponding values of ω (in degrees) as deduced from relation (A.3).

In botany, a simple quantity to measure on cuts of apices is precisely this sustaining angle ω (as was first done by Snow & Snow, 1993 and 1952). Such measurements could then be compared with the values of ω given here. A difficulty only arises in the cases pointed out by Wardlaw (1968), where the apparent size of the primordia is much smaller than the size of its zone of inhibiting influence (as seen in e.g. ferns). The angle to be measured in this case is that obtained by enlarging all primordia so that they come into contact.

For comparison with Part I, we will also give the parameter $G = VT/R_0$ where T is the mean time of appearance between primordia. As discussed in Part (I), this parameter G is linked to a, (Richards' plastochrone ratio (1951) by $a = \exp(G)$ and can be deduced from measurements on the positions of the primordia. Note that a and G are the ratio of two lengths measured on the plane.

2.3. SIMULATIONS SET-UP

The numerical simulations were done on Macintosh computers MIIfx, Quadra 950 and Quadra 840 av. The programme was written in Think Pascal (21 pages, mostly used for the presentation). The simulations of the hypotheses of Snow & Snow are much more time consuming than those of Hofmeister, because the time at which the new element will appear is unknown. But it is possible to improve the computation efficiency by using an estimate of the time of appearance. This estimate is obtained by first measuring, at some time, the minimal energy. Then we use the oversimplification that this energy is because of the effect of one single particle. With the energy profile of one element, we can then estimate the distance of this virtual particle. We then get an estimate of the time needed to reduce the energy to the threshold by advection of this particle. For each new estimate, we still have to find the minimum of the energy on the circle (as in Part I), and to see whether it is below or above the threshold. After only a few tries the right time is found. This time t is defined as being that for which the minimum E is below the threshold, but by so little that the minimum at the previous time step precision $(t - \Delta t)$ is above the threshold. We used a typical time step precision $V\Delta t/R_0 = 0.0002$. Once the programme optimized, typically 4 min were enough to compute the appearance of 150 elements.

2.4. RUNNING THE SIMULATIONS

The results of iterative systems depend in part on the initial conditions. As we will see, for a given value of the parameter Γ, the mode which will actually be observed can depend on the transient by which the

value of Γ has been reached. In order to be exhaustive several types of simulations were done.

We first investigated the modes obtained during a quasi-steady decrease of the parameter Γ. The following procedure was used. We started from a large enough value of Γ and then decreased it step by step. For each Γ we let n consecutive particles appear. In the simulations presented below, n was as large as 150. We then used the positions of the last deposited particles (e.g. 20) at a value of Γ as initial conditions for the next smaller value of Γ. (The number of values of Γ explored was of the order of 200.)

For most values of Γ this procedure was sufficient to reach steady regimes of the iteration. For some values of Γ near a transition, however, we had to do simulations with a very large number of particles (e.g. 500) to reach the steady regime. This is irrelevant from the botanical point of view and was only done to get the asymptotically stable mode.

In the second type of simulation we forced the system by initially imposing a few elements, having the expected symmetry and position, and observed whether or not the pattern could keep growing. If the pattern stabilized, we again used the last particles as initial conditions for the next simulation. In that way we explored the main secondary modes of the iteration.

In a third type of simulation we also explored the patterns in ranges of values of Γ where they were unstable. For this purpose we used as initial conditions elements placed at their expected position (approximated from the average divergence and average plastochrone) at the previous value Γ. The patterns usually started growing in this mode and only destabilized later. It was thus possible to obtain a value of φ and T for the new value of Γ before this destabilization. This procedure could be used for both unstable spiral and whorled modes. In this latter case the imposed initial elements were placed with the positions of a perfect whorled pattern and the previous average plastochrone.

Finally we will present in the third article (Douady & Couder, 1996b) various sets of simulations in which our aim was to explore the regimes that were most likely to be observed in botany. For this purpose we explored the patterns obtained with realistic initial conditions when the control parameter underwent a time evolution $\Gamma(t)$ of the type observed in plants.

3. Results. The Permanent Regimes: Spontaneous Formation of a Time Periodicity

Although we performed simulations for many values of $1/N$ and α we will first limit ourselves to the discussion of a single case with a folioid parameter $1/N=3$ and a stiff interaction $\alpha=8$. Then we will compare it to other cases and discuss the effect of conicity and stiffness.

The first result of our simulations is that, for all values of Γ, steady regimes of the iterative system can be obtained. The number of different possible modes is larger than in Hofmeister's type of simulation and involves both spiral and whorled modes of growth.

As there is a large number of possible patterns we will, for clarity, first limit ourselves to those that are reached during a very slow decrease of the control parameter Γ (Fig. 4). Afterwards (Section 3.3) we will discuss the other possible organizations.

3.1. DISTICHOUS AND FIRST SPIRAL MODES

The steady regimes of the iterative system can first be characterized by their periodicity in time. For each value of the imposed control parameter Γ, we plotted the observed time intervals δt between the formation of two successive primordia. The results are given on Fig. 4(a) for $1/N=3$ and $\alpha=8$.

For large values of Γ, this time interval has a single value $\delta t=T$; during each period there is formation of a single new primordium. The observed period T (or plastochrone) varies roughly as the square of Γ [cf Fig. 4(a)]. This simple dependence will be discussed in more detail in Section 4.1.

The results can be first studied by plotting the divergence angles between two successive particles as a function of Γ [Fig. 4(b)] or as a function of the sustaining angle ω [Fig. 4(c)]. For the sake of comparison with the results of Part I we can finally plot the divergence φ as a function of $G=VT/R_0$ [Fig. 4(d)]. In the present simulation R_0 and $V(R_0)$ are fixed so that G is simply proportional to the observed periodicity T. The essential difference with Part (I) is that the value of this plastochrone T is no longer imposed but results from the dynamics of the iteration at a chosen value of Γ. As this periodicity T is observed to vary roughly as the square of Γ, however, the two figures 4(b) and 4(d) have a similar structure. Down to $\Gamma=1.89$ (or $\omega=114^\circ$, giving $G=0.155$) the evolution of φ is also similar to the main branch of the diagram shown in Fig. 4, part I (Douady & Couder, 1996a), even though the threshold values for G are shifted by the effect of conicity (see Section 4.4). We obtain the distichous mode for large Γ (or G), the symmetry breaking bifurcation at Γ_c (or G_c), then an imperfect bifurcation leading from a spiral mode (1,2) to (2,3). This result shows that imposing a regular plastochrone T, as done in Hofmeister's set of hypotheses, was superfluous: the system itself can spontaneously generate its own periodicity.

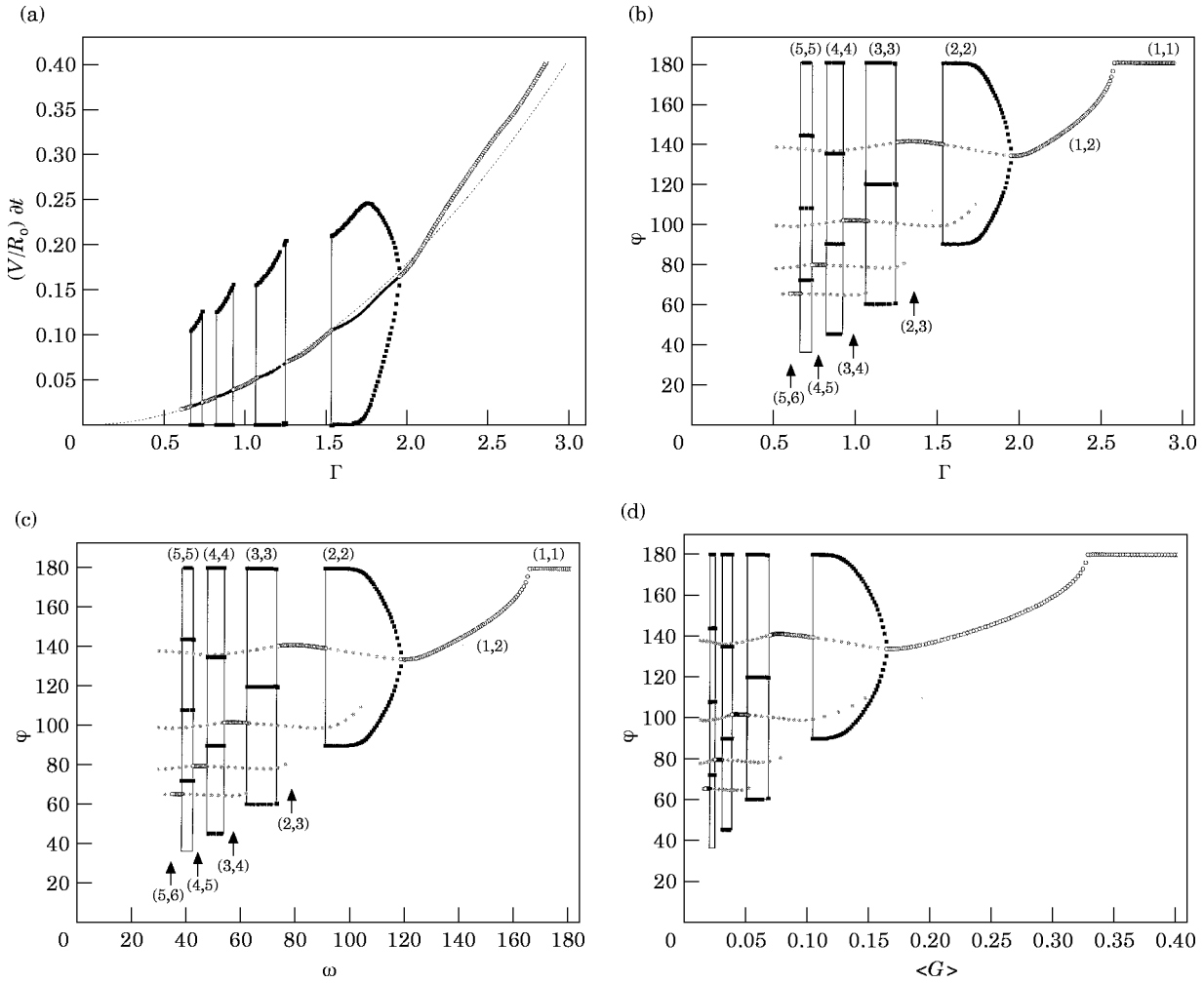

FIG. 4. Characteristics of the patterns obtained with a conicity $1/N = 3$ and a stiffness $\alpha = 8$. On each of these curves a point represents a steady regime (after approximately 150 particles). The open circles (○) correspond to steady spiral organizations and the black squares (■) to the stable whorled modes. These modes were those obtained in a slow decrease of Γ. For the clarity of the diagram we have also represented (grey points on b, c and d) organizations obtained by a forcing using specific initial conditions. (a) The time intervals δt separating the appearance of successive primordia as a function of Γ. In this diagram δt is normalized by V/R_0. In the regions of spiral organization δt has only one value, the plastochrone T so that $V\delta t/R_0 = VT/R_0 = G$, the logarithm of the plastochrone ratio. In the others δt is multi-valued and one of the value tends towards zero. This is because of the quasi simultaneous formation of several elements in the whorled modes. In these regions the black diamonds show the average periodicity $\langle G \rangle = (V/R_0)T_n/n$. The dotted line shows the curve $G = \beta/8N\Gamma^2$ with $\beta = 1.08$. (b) Diagram of the steady divergence φ as a function of Γ. The regions in which φ is multi-valued correspond to the whorled modes. (c) Same results as (b) but φ is given as a function of the sustaining angle ω. (d) Same results as (b and c) but with φ shown as a function of the average plastochrone ratio $\langle G \rangle$. The thresholds values are shifted relatively to the plane case of Part (I).

Figure 5(a) shows a pattern obtained at $\Gamma = 1.25$ ($\omega = 73.3°$). If we want to draw the parastichies on such a pattern we can use two different criteria. Either we link each element with its nearest neighbours or we link it to the elements with which it is in contact. Dynamically, the organization of the elements comes from the "contact" because of their repulsive field. For this reason the important parastichies are the contact ones. In all radial configurations, however, if the elements have a constant size, the advection of the elements pulls them apart so that they lose contact with each other. The dynamically important parastichies are thus only visible near the apex. They are easier to see in the cases (shown in Fig. 9 and discussed in Section 4.5) where the elements grow in size proportionally to their distance from the centre. In this case the contact between the elements is maintained so that they are visible everywhere and not only close to the apex border. This will be used for a discussion of the space filling characteristics of the patterns.

3.2. WHORLED MODES

A constant time interval between the formation of successive elements is not, however, the only type of periodicity observed. Figure 4(a) shows that there are ranges of values of Γ for which the time intervals can take two different values: $\delta t \approx 0$ and $\delta t = T_n$. In these regimes a number n elements are formed practically simultaneously ($\delta t \approx 0$) and a period T_n separates their formation from that of the next group. Inspection of the corresponding spatial structures (see Fig. 6) shows that at each period n elements, evenly spaced on the circle, form in directions which bisect the angles formed by the direction of the elements of the previous period. These modes thus have the spatial dispositions observed in the botanical alternate whorled modes in which n leaves form simultaneously at successive nodes along the stem.

In the $\varphi(\Gamma)$ diagrams [Fig. 4(b)] the ranges of existence of the whorled modes are characterized by regions where φ is multi-valued. Between elements of the same node these angles are of the type $\varphi = 2p(\pi/n)$ where p is an integer ($0 < p < n$). The divergences between the last element of a node and the first element of the following node are generally close to $\varphi = (2p+1)\pi/n$. As we will see it is also possible to obtain regimes with different values of these latter angles. They correspond to either imperfect whorls (Section 4.2) or to multijugate spirals (Section 3.3).

For all these modes we can introduce an averaged periodicity $\langle T \rangle$. If the whorls are perfect (the several elements of the whorls are created exactly at the same time, $\delta t = 0$) then $\langle T \rangle = T_n/n$. The value of this average is found to be very close to the periodicity of the neighbouring spiral modes, and of the quadratic dependence $T(\Gamma)$ [Fig. 4(a)]. Finally it is possible to represent the whorled modes (n, n) in the $\varphi(G)$ diagrams by replacing G by its average $\langle G \rangle = V\langle T \rangle / R_0$. This is done on Fig. 4(d): the ranges of existence of the whorled modes are again characterized by regions where φ is multi-valued. For simplicity we will, in the following, omit the average symbol: whenever a plastochrone ratio will be used for a whorled mode it will be understood to be an average one.

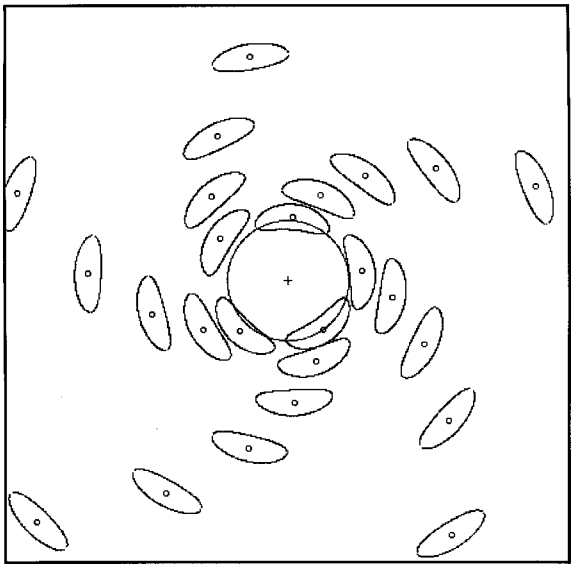

FIG. 5. A spiral mode (2, 3, 5) obtained in the case with conicity $1/N = 3$ with stiffness $\alpha = 8$ for $\Gamma = 1.25$. Each particle is represented by the isopotential that it generates and which corresponds to its core. It has a orthoradial length $l_1 = d_0(\sin(\Psi/2)^{-1/2}$ and a radial size $l_2 = d_0(\sin(\Psi/2)^{1/2}$. The average $(l_1 l_2)^{1/2}$ is d_0.

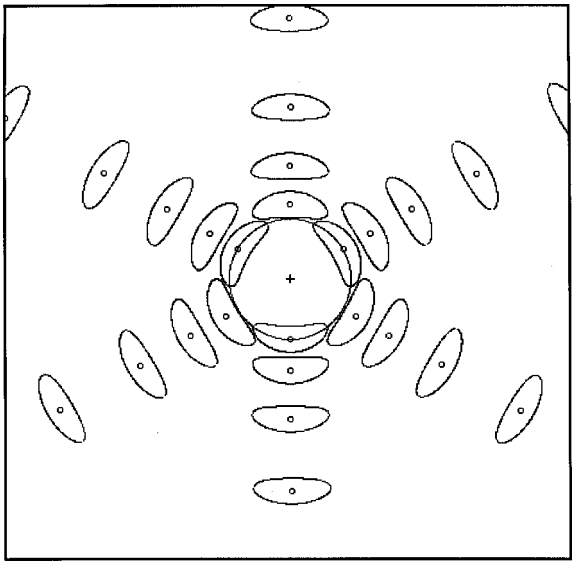

FIG. 6. A whorled mode (3, 3) obtained with the same parameters as in Fig. 5: conicity $1/N = 3$, stiffness $\alpha = 8$ and $\Gamma = 1.256$ ($\omega = 77.8°$).

In the case presented in Fig. 4, where $\Gamma = 1.89$ down to $\Gamma = 1.7$ (i.e. from $\omega = 114°$ to $\omega = 101°$ and from $G = 0.155$ to $G = 0.121$), a spontaneous and progressive transition to the opposite decussate phyllotaxy (2, 2) exists which remains stable down to $\Gamma = 1.52$ ($\omega = 90.1°$, $G = 0.104$) where the system returns to a spiral mode (3, 5) situated on the main spiral branch (Fig. 5). Then at $\Gamma = 1.25$ ($\omega = 73.4$) the system forms a trimerous whorled pattern (3, 3) shown in Fig. 6. At $\Gamma = 1.07$ ($\omega = 62°$) it returns to a spiral mode (3, 4) situated on the first secondary branch. During the further quasi-static decrease of Γ there will be successive transitions to (4, 4) then to (4, 5) etc. This type of transition then repeats itself and the system goes from a whorled mode (i, i) to a spiral $(i, i+1)$ then to $(i+1, i+1)$. The botanical relevance of such transitions will be discussed in the

third article (Douady & Couder, 1996b). We can note that the lower limit of existence of a whorled modes (i, i) corresponds roughly to values $\omega \sim 360°/2i$, as could be expected from the geometry of the patterns.

3.3. OTHER MODES: SECONDARY SPIRALS, BIJUGATE AND MULTIJUGATE SPIRAL MODES

Either using specific initial conditions or specific time evolutions of $\Gamma(t)$, other modes of organization could be obtained which were mostly omitted in Fig. 4. They first consist of all the secondary spiral organizations obtained in Part I, in which the parastichy orders are numbers from secondary Fibonacci-like series built from different initial integers such as (1, 3, 4, 7, 11, . . .), (1, 4, 5, 9, 14, . . .), (2, 5, 7, 12, . . .) etc. each converging towards a limit divergence angle with an irrational value $\varphi = 99.502°$, $\varphi = 77.955°$, $\varphi = 151.135°$ etc.

Apart from these spiral modes and the whorled modes it is also possible to get patterns called multijugate by botanists. The easiest to obtain is reached when a rapid decrease of Γ is applied to a decussate mode. Below a threshold value, while the two elements of a whorl remain opposite ($\varphi = \pi$), the angle between two elements of different whorls can take two values $\varphi' < \pi/2$ or $\varphi' > \pi/2$ so that two branches are observed in the $\varphi(\Gamma)$ diagram (see Fig. 7). The patterns observed along these curves have parastichy order of the type $(2i, 2j)$, where i and j are numbers of the main Fibonacci series. These are thus bijugate modes. The branches that we observe are related to the possible divergences obtained by Erickson (1973) when he extended van Iterson's geometric calculations to bijugate modes. In the low Γ region the bijugate organization is stable so that the main bijugate branch is easy to follow during a steady decrease of Γ. This is not true in the region where the transition from decussate to bijugate (2, 4) occurs. There is a range of values in Γ in which these solutions are unstable. This is the reason for the return to the spiral mode (2, 3) normally observed in a slow decrease of Γ as described above.

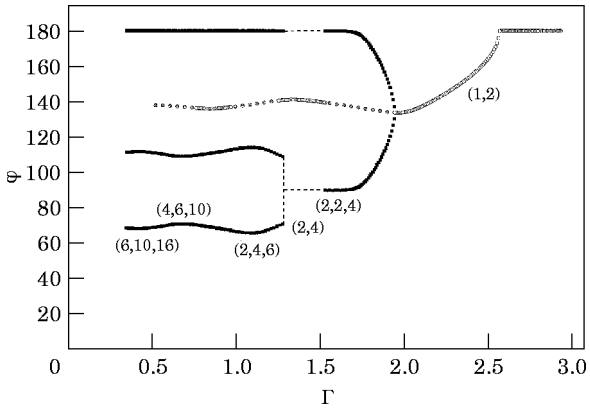

FIG. 7. Diagram of the divergence φ as a function of Γ showing the position of the bijugate branch relative to the decussate region. Dotted lines have been drawn in the unstable region separating the decussate region from the bijugate one.

In more general terms the opposite decussate mode can be considered as the distichous mode repeated twice. A bijugate mode 2 (i, j) also corresponds to the normal spiral mode (i, j) repeated twice. As a result a complete diagram with all the secondary Fibonacci branches could be found for the bijugate modes. Similarly, all the whorled modes (n, n) can be seen as distichous modes repeated n times and all the multijugate modes $n(i, j)$ thus form similar diagrams starting from their respective whorled mode. With increasing order these modes become more difficult to reach in the simulation, they are also rarer in botany. Of the whorled modes the most usual is the decussate phyllotaxy and the most common cases of multijugate organization are the bijugate modes of the main Fibonacci branch (2, 2, 4, 6, 10, 16, 26 etc.) drawn in Fig. 7.

4. Discussion: Selection of Modes and Transition Between Modes

We will show in this section that all the previous results can be explained if the relative compactness of the different modes is considered. We will also discuss the respective selection of spiral or whorled modes depending on the conicity, and on the stiffness of the primordia interaction.

4.1. THE MEAN PERIODICITY OF THE ITERATION AND THE COMPACTNESS OF THE PACKING

In order to understand the relative stability of the different modes we can revisit the dependence of the mean time of appearance of a new primordium $\langle T \rangle$ on the imposed Γ. The plot given in Fig. 4(a) shows that on the average $\langle T \rangle \propto \Gamma^2$. This quadratic mean dependence of $T(\Gamma)$ and the fluctuations around it can be directly related to the spatial organization of the pattern. Let us consider all the elements formed between a time t_0 and a time $t_0 + \Delta t$. If exponential growth is assumed, they are all located at time $t_0 + \Delta t$ in an annulus of inner radius R_0 and outer radius $R_0 \exp(V\Delta t/R_0)$. The area of this annulus is

$$\Delta S = \pi(R_0^2 \exp(2V\Delta t/R_0) - R_0^2) \tag{8}$$

For small Δt it reduces to

$$\Delta S \approx \pi R_0^2 (2V\Delta t/R_0) \tag{9}$$

The primordia present in this area are those formed

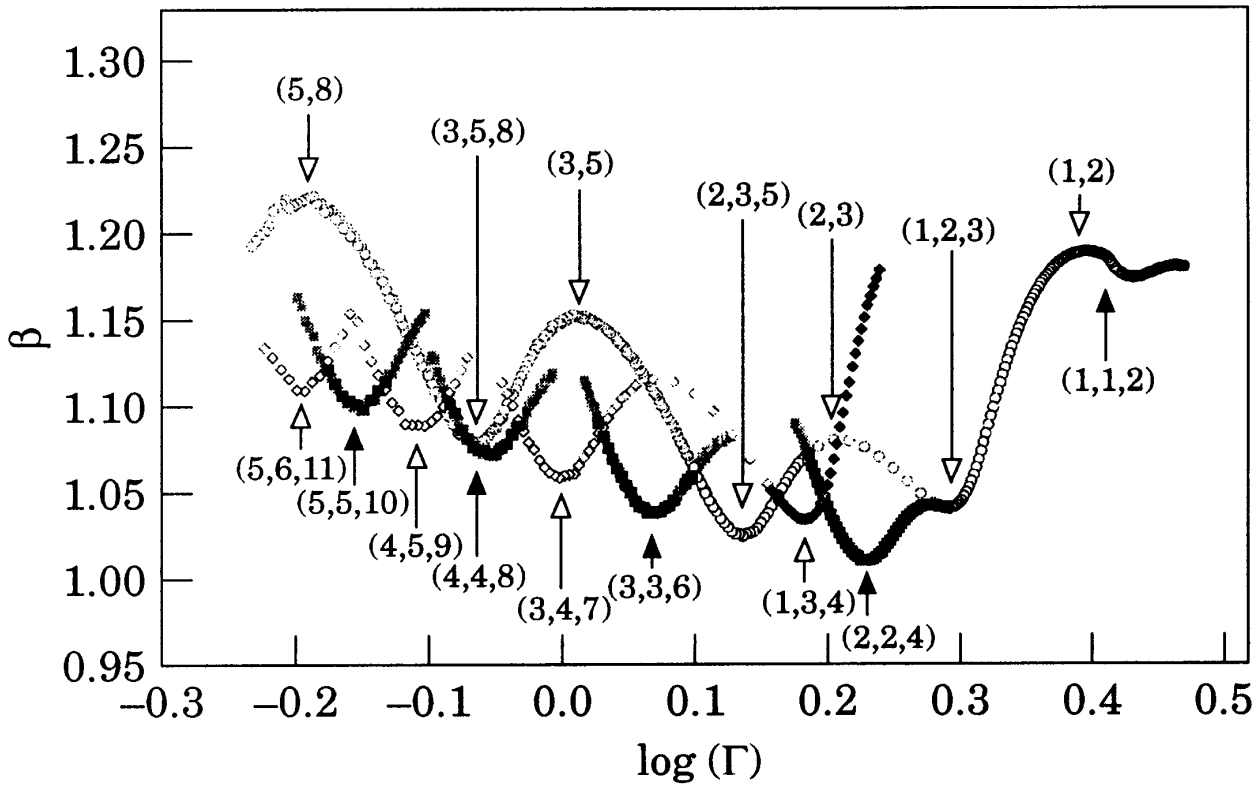

FIG. 8. The compactness of the piling can be defined by the parameter $\beta = 8\langle G\rangle/(N\Gamma^2)$. (The smaller β the more compact the piling). Its variation is shown here as a function of log(Γ) (in the case $1/N = 3$ and $\alpha = 8$ of Fig. 4). The oscillations observed here correspond to the small fluctuations around the dashed curve of the mean periodicity $\langle T\rangle$ observed in Fig. 4(a). The open circles (○) corresponds to the main Fibonacci branch (in grey for the unstable states). Along the curve representing the main Fibonacci series, the successive increase in the order of the parastichies results here into an oscillation of β. It is minimum at the transitions from (i, j) to $(j, i+j)$ when the pattern has, on the cone, a local hexagonal piling [denoted $(i, j, i+j)$]. It is maximum in the region (i, j) where the pattern is a square tiling (on the cone). The black squares (■) correspond to the successive whorled modes. As for the spirals, β is also minimum when the whorled patterns have, on the cone, a local hexagonal piling [noted $(n, n, 2n)$]. The grey diamonds correspond to the modes (1, 3) and (1, 3, 4) of the Lucas series which are obtained with specific initial conditions. The important feature of this figure is that the stable configurations for long iterations at a given value of the control parameter Γ are those with the smallest β.

in the time interval Δt: their number is simply $\Delta t/\langle T\rangle$. If they are disks of radius $d_0/2$ the total area that these disks cover is

$$\Delta S' = (\pi d_0^2/4)(\Delta t/\langle T\rangle). \tag{10}$$

We can define the ratio $\beta = \Delta S/\Delta S'$. It is a function which represents the compactness of the packing. The smaller its value, the denser the piling. Equating $\Delta S = \beta \Delta S'$ we find:

$$\beta = 8R_0 V\langle T\rangle/d_0^2 = 8\langle G\rangle(R_0/d_0)^2 \tag{11}$$

or, using the definition (7):

$$\langle G\rangle = (\beta/8)N\Gamma^2 \tag{12}$$

This relation yields that, for a given conicity N, if the compactness β was constant, we would have: $\langle G\rangle \propto \Gamma^2$ which is roughly observed in Fig. 4(a). The curve, however, has small fluctuations around this quadratic fit. These deviations are caused by the fact that β is in reality a function of Γ.

The $\beta(\log \Gamma)$ dependence shown in Fig. 8 forms a distinct branch for each type of pattern. It is to be noted that each of these branches has a minimum, and that the region for which the corresponding pattern is spontaneously observed corresponds to the vicinity of these minima. To the succession of minima of the $\beta(\Gamma)$ curves corresponds the succession of observed patterns. It is worth noting that modes other than the most stable are represented on Fig. 8: they were generally obtained by initially forcing the structure of the pattern.

The oscillations around the quadratic dependence can be understood as resulting from variations of compactness of the packing which is measured by β. Let us, for instance, examine the variation of $\beta(\Gamma)$ along the main Fibonacci branch. Figure 8 shows that

it forms a curve oscillating between lower and higher limits. Except for large values of Γ, the amplitude of the oscillations remains roughly constant when the Fibonacci order increases. Comparison with Fig. 4(b) shows that the minima of $\beta(\Gamma)$ occur for the values of Γ where there is transition from a mode (i, j) to a mode $(j, i+j)$.

Although the piling is the same near the apex, the dynamically important parastichies are better observed in the case where the elements grow in size proportionally to their distance from the centre. For this reason the patterns shown on Fig. 9 have been taken in the case of elements growing in size discussed below (see Section 4.5 and Fig. 13). Figure 9(a) shows such a lattice obtained at the transition between (2, 3) and (3, 5). Each folioid is in contact with six neighbours so that there are three contact parastichies, noted $(i, j, i+j)$. This is the projection of a

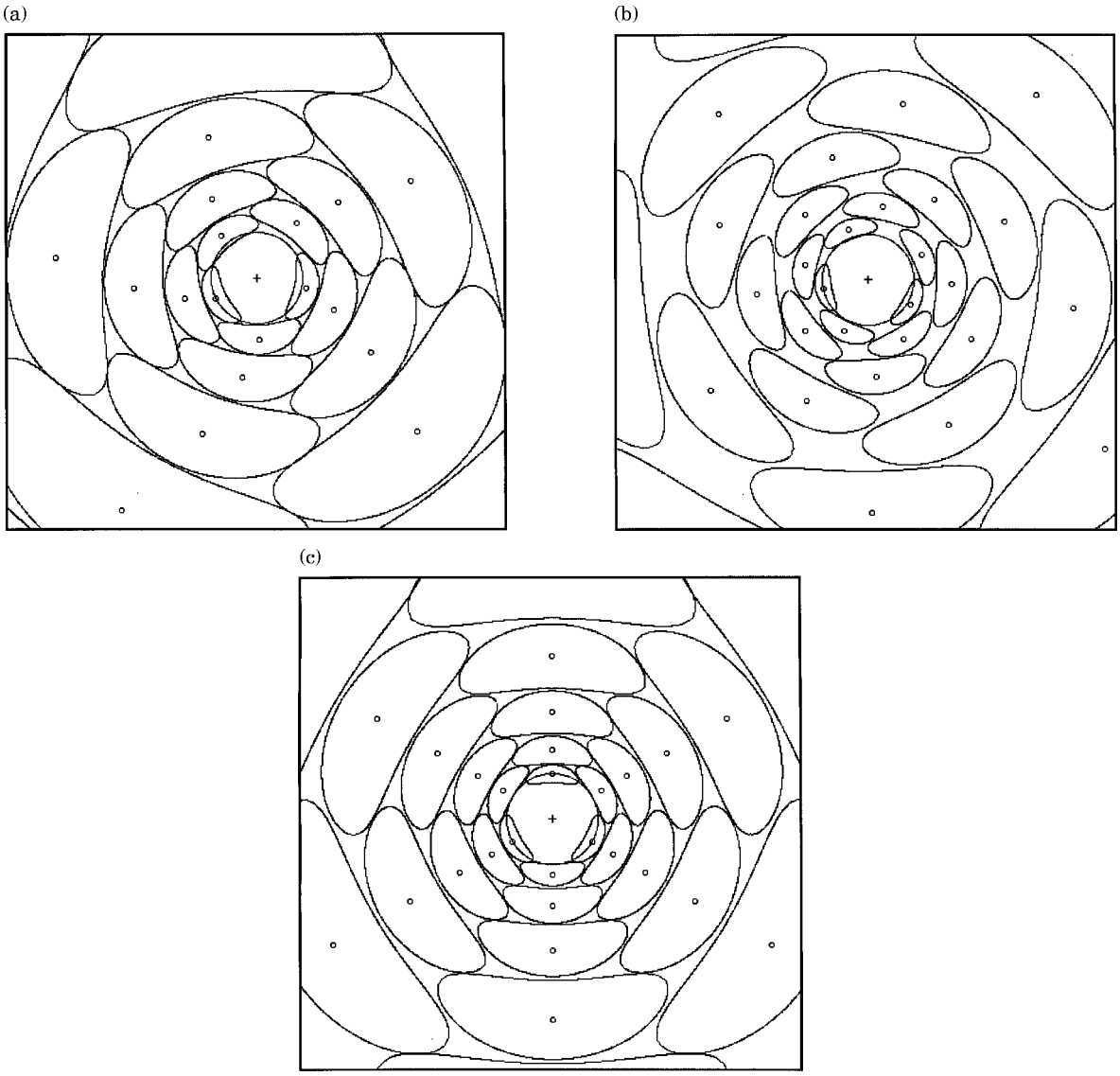

FIG. 9. The local piling of three patterns obtained with $1/N=3$ and $\alpha=8$. The important set of parastichies are the contact ones. In most of our simulations the "size" of the elements was constant so that there was only contact in the region where they form. In order to make the contact parastichies more visible we show here patterns obtained in simulations in which the elements grow in size during their radial motion (see their $\varphi(\Gamma)$ plot of Fig. 13). (a) Lattice obtained at a value $\Gamma=1.126$ ($\omega=68.5°$) corresponding to a Fibonacci spiral mode (2, 3, 5) in Fig. 13. Three sets of contact parastichies are clearly seen of order two, three and five respectively. This corresponds to a minimum of $\beta(\Gamma)$ and to a lattice which is hexagonal on the surface of the cone. (b) A spiral lattice obtained at a value of $\Gamma=0.935$ ($\omega=55.7°$). It corresponds to a mode (3, 5) as seen here by the two contact parastichies. At this value $\beta(\Gamma)$ is close to a maximum: the large space lost between the primordia is easily seen. This disposition corresponds to a lattice which is almost square on the cone and which is unstable. The pattern shown here was only observed as a transient. (c) In the same range of values of Γ, the stable organization is the three-fold whorled lattice (see Fig. 13). For $\Gamma=0.99$ ($\omega=59.3°$), β of this mode is close to a minimum. Three sets (3, 3, 6) of contact parastichies are observed. The corresponding lattice on the cone is hexagonal.

configuration which, on the surface of the cone, is a nearly hexagonal packing of disks, with parastichies intersecting at angles 60° and 120°. It is well known that in two dimensions hexagonal packings provide the largest compactness. The regions of transition $(i, j, i+j)$ correspond to minima of $\beta(\Gamma)$.

In contrast, halfway between two transitions, the pattern only has two parastichies (i, j). An example is the spiral mode shown in Fig. 9(b) where the Fibonacci order is (3, 5) and each element is in contact with only four nearest neighbours. On the conical surface these parastichies would intersect approximately at right angles and the disks would thus have a square piling. This corresponds to the worst possible packing of touching disks in two dimensions, and to a maximum of $\beta(\Gamma)$ (Fig. 8). This mode (3, 5) is actually not stable: at this value of Γ it is the whorled mode (3, 3) that is normally selected (see Fig. 13). The arrangement shown on Fig. 9(b) could only be obtained transitorily and from well chosen initial conditions.

If we now examine the patterns of the whorled modes at the values of Γ of their minimum β they can be seen as having three parastichies, so that they have locally a hexagonal packing on the cone. This can be observed in Fig. 9(c) where a whorled mode (3, 3) is shown for a value of Γ corresponding to its minimum β. Clearly each element has six nearest neighbours and the corresponding "parastichies" are in fact (3, 3, 6). We can note that, from a geometrical point of view, there are in principle two possible whorled patterns with a hexagonal packing. The first one, at larger Γ, is when the primordia of the same whorl are in contact, so it can be noted $(0, n, n)$, while the second case, at lower Γ, occurs when the primordia of a given whorl are in contact with those of the second previous whorl. In this case there are perfect orthostiches and the pattern can be noted $(n, n, 2n)$. A result of our simulation is that only the whorled modes close to this latter case are obtained, the other mode was never observed.

These results on the oscillation of the compacity can be compared to those of geometric calculations. The packing efficiency of phyllotactic patterns was first investigated by Ridley (1986) who limited himself to varying the distances of elements set with a divergence having a fixed value. More recently, the theoretical values of the coverage β were computed by Douady (1996) in the case of disks disposed on the surface of a cylinder (a geometry first introduced by van Iterson, 1907). In this case it is easy to find the efficiency of regular packings. The result is that $\beta = 2\sqrt{3}/\pi \approx 1{,}103$ for a hexagonal lattice and $\beta = 4/\pi \approx 1{,}273$ for a square one. In the limit where d_0/R_0 is small (high order modes), the coverage of a cone by disks is not very different from that of a cylinder of perimeter $2\pi R_0$ with disks a diameter d_0. We find a reasonable agreement: the oscillations of $\beta(\log \Gamma)$ between an upper and a lower envelope is well understood by this model. When d_0 becomes of the same order as R_0, however, the radial character of the geometry near the the tip becomes dominant. The minima of the packing are then different, as will be discussed below (end of Section 4.4).

4.2. THE TRANSITIONS FROM ONE MODE TO ANOTHER

The transitions between different modes of organization will have a fundamental importance for the understanding of botanical data, and as such will be examined in detail in Part III. Here we will limit ourselves to the dynamical characteristics of these transitions. Three types of transitions can be observed in the diagrams shown above (Figs 4 and 7).

The first type of transition characterizes the transition (i, j) to $(j, i+j)$ (with $i<j$) between spiral modes with parastichy numbers of the same Fibonacci series. The situation in this case is the same as in Part I: the transition is smooth and there is a continuum of intermediate steady states. All the curves $[\varphi(\Gamma), \varphi(\langle G \rangle), \beta(\Gamma)]$ are smooth and continuous in the region of transition [see, for instance, the transition between (2, 3) and (3, 5)]. Similarly continuous is the transition from the mode (1, 2) to the decussate mode (2, 2) which occurs through a series of stable intermediate states. This particular transition will be discussed in detail in the third article of this series.

A second type of transition is observed in Fig. 4. For decreasing Γ, it corresponds to the successive transitions from the spiral patterns $(j-1, j)$ to the whorled modes (j, j), as well as the transitions from the whorled mode (j, j) to the spiral patterns $(j, j+1)$ [with the exception of the transition from (1, 2) to (2, 2) mentioned above]. Whether decreasing or increasing values of Γ are imposed, the transitions are identical, provided the number of iterations is large. Contrary to the previous case, there is no continuity in the steady values of the divergence [$\varphi(\Gamma)$ or $\varphi(\langle G \rangle)$] at the transition [Figs 4(b) and (d)]. The steady value of the angle goes for instance from the value φ_s for the spiral pattern $(j-1, j)$ to the values $\{\varphi = \pi p/n, 0 < p \leqslant n\}$ of the whorled mode (j, j). As for the curve $\beta(\Gamma)$ (Fig. 8) it remains continuous, having only a sudden change in the sign of its slope when passing from one mode to the other. This corresponds to the crossing of two different curves $\beta(\Gamma)$, corresponding respectively to the two modes. The transition thus occurs at the value of $\beta(\Gamma)$ for

which the two curves intersect, in other words, when the two modes have the same compactness.

For a value of Γ where a mode is unstable, the transformation of this mode into the second is continuous: the angles and the time from one element to the next change only slightly at each iteration. Near the value of Γ for the intersection, a very large number of iterations (up to several hundred) are needed for the transformation to be completed. This is a general characteristic for second order transitions of dynamical systems: the time needed to complete the transformation becomes infinite at the transition value. As a consequence we observe a delay in the transition if only a small number of elements is deposited for each value of Γ. Unstable states can thus be obtained transitorily on both sides of the ideal transition point (see the grey points on Fig. 8).

In crystallographic terms, these transitions correspond to the formation of an additional parastichy. The transient thus corresponds to the formation of a crystallographic dislocation in the initial pattern as described by Zagorska-Marek (1987) and by Meicenheimer & Zagorska-Marek (1989).

Finally, it is worth noting that if the value of Γ is changed rapidly, there exists the possibility that a spiral mode does not have the time to transform, thus skipping the whorled organization and going directly from a stable spiral mode to the next on the same branch. This is important for the possibility of the build up of high order spiral phyllotaxy as will be discussed in Part III.

A third type of transition exists: as shown in Part (I) the spiral modes form separate branches of the $\varphi(G)$ diagram. All these modes, except those of the main Fibonacci branch, cease to exist above an upper limit value of G. With the Snows' rule we find a similar structure: on the $\varphi(\Gamma)$ [or $\varphi(\langle G \rangle)$] diagram, each of the spiral branches (except the main one) vanishes above a limit value of Γ [Fig. 4(b)]. When Γ, being increased, reaches this limit, the pattern does not change continuously: a new element appears in a place very different from the normal one and the pattern breaks down and restabilizes rapidly on a new mode. This can be understood on the plot $\beta(\Gamma)$ (see the grey diamonds on Fig. 8). The extremities of the secondary spiral branches always correspond to a large value of $\beta(\Gamma)$. In the transition $\beta(\Gamma)$ decreases strongly as the pattern increases the compactness of its packing. It is surprising that, before the transition, the spiral pattern can remain stable, although far from optimum. The metastability of the pattern before the transition suggests that there is a topological hindrance to an earlier transition.

Other transitions can be more complex. They can be interpreted as the destabilization of one mode to a second, which in turn is unstable to a third. For instance, increasing Γ, a spiral mode (3, 4) becomes unstable and gives rise to a transient whorled mode (3, 3), which in turn destabilizes to the mode (2, 3). Such types of transitions are only possible with the Snow & Snow rule (see Part I).

We will address in Part III the question of the botanical relevance of all these possible transitions.

4.3. THE SELECTION OF ONE MODE WITH RESPECT TO ANOTHER

The main interest in measuring the compactness β is that it provides a criterion for the relative selection between the whorled modes and the spiral ones. In general, the comparison of the diagrams of Fig. 4 with the $\beta(\Gamma)$ dependence of Fig. 8 shows that generally at a given Γ, when several modes are possible, the one with the smallest value of β is stable. In the particular case of the whorled modes (i, i) and of the related spiral modes $[(i, i+1)$ or $(i-1, i)]$, the stable mode at a given value of Γ is the mode with the smallest $\beta(\Gamma)$. This means that, in general terms, the iterative system tends to create the structure with the largest density.

Finally the transitions occurring at the upper limit of the secondary spiral modes (for increasing Γ) show that compactness is not the only criterion of selection. These modes, just before becoming unstable, can present a large β (see Fig. 8). The transition between one mode and another is thus not only a problem of the optimization of the packing. It is also linked with topological possibilities of a continuous deformation of the pattern from the initial mode to the final one. For the first and second types of transition described above, this topological continuity is clearly observed. The transition thus occurs when the new mode has a denser packing than the previous one. In contrast, such a topological continuity does not exist for the third type of transition. This is why the initial mode remains stable even though being far from optimum, and why the following transition is brutal.

In practice, some transitions from one mode to another can last during a large number of iterations. In spite of their theoretical interest such transitions may be meaningless from the botanical point of view. In botany the production of a very large number of elements is the exception rather than the rule so that some transitions can fail to occur. These problems will be discussed in the third article (Douady & Couder, 1996b).

Finally we can remark that with Hofmeister's rule (Douady & Couder, 1996a), the time of formation of

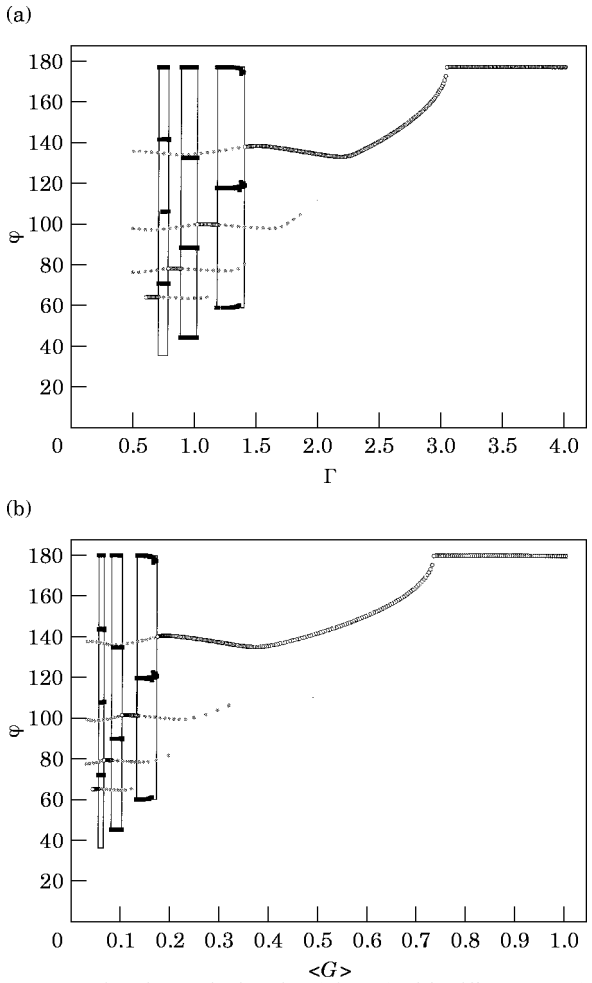

FIG. 10. Plane isotropic situation ($1/N=1$) with stiffness $\alpha=8$. (a) Diagram of the divergence φ as a function of Γ. (b) Diagram of φ as a function of $\langle G\rangle$. The conventions are the same as for Fig. 4. Note the absence of the decussate mode (2, 2) which is not observed spontaneously for these values of the parameter. The spiral modes have the same $\varphi(G)$ dependence as was found in part I when stiff interactions were used.

the elements was imposed and could not fluctuate. The effect of the variation in the compactness of the packing was thus different. It affected the energy at which the elements were formed (or in other words their size d_0 or Γ). Similar fluctuations could thus have been detected if this energy (or Γ) had been investigated as a function of G. The condition of selection would then have been to optimize the size of the elements (i.e. to minimize the energy). For simplicity, this condition of optimization of the packing was not emphasized in Part I, although it explains the selection of the branch following the Fibonacci rule in the imperfect bifurcations (Douady, 1994). This is the selection mechanism which was used in a related problem by Levitov (1991a, b). This global selection can be seen as different, while being the consequence of the local dynamical optimization occurring in botanical growth.

Finally we can note that this selection of the densest patterns contradicts a hypothesis of van Iterson (1907). Remarking (as Bravais before him) that the divergence φ always seemed to be close to Φ he proposed that, along the oscillating branch of his diagram φ(b), the most stable regions corresponded to the square patterns. These organizations, being found halfway between two bifurcations, correspond to the region of each branch where φ is closest to Φ [see Fig. 4(b)]. We believe that the proximity of φ to Φ appears surprising only because the parastichy order tends to be underestimated, an effect caused by the secondary elongation already discussed in Part I (Section 5.5-ii).

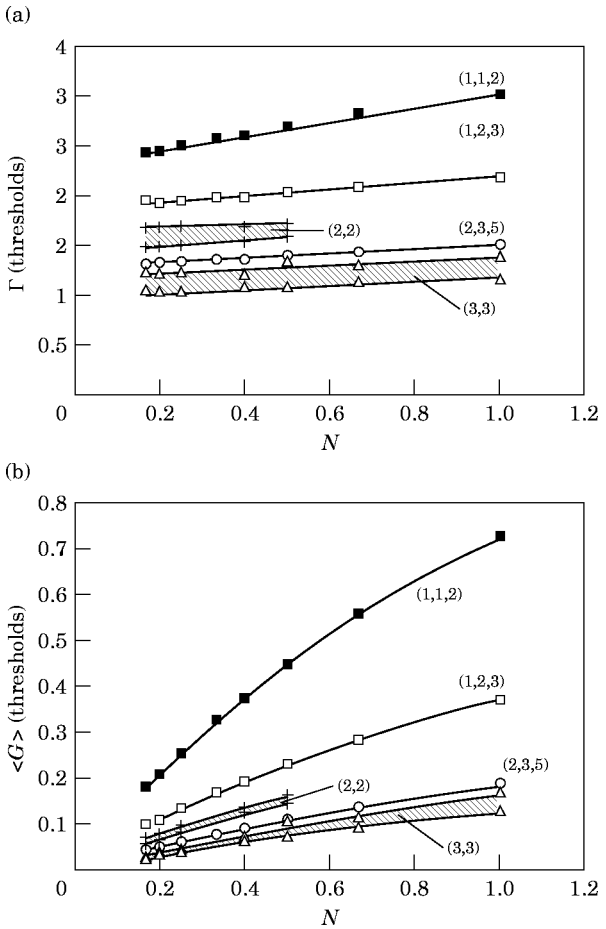

FIG. 11. The evolution of the first thresholds as a function of the conicity $1/N$. (a) Evolution of Γ. Black squares (■): transition from the distichous mode to the spiral (1, 2). White squares (□): transition from (1, 2) to (2, 3). Crossed squares (⊞): transition from (2, 3) to (3, 5). The two shaded areas are the ranges of existence of the perfect decussate mode [limited by crosses (+)] and of the trimerous whorls [limited by triangles (△)]. Except for the first two transitions the threshold values of Γ are only weakly dependent on N. (b) Evolution of the values of $\langle G\rangle$ at the thresholds.

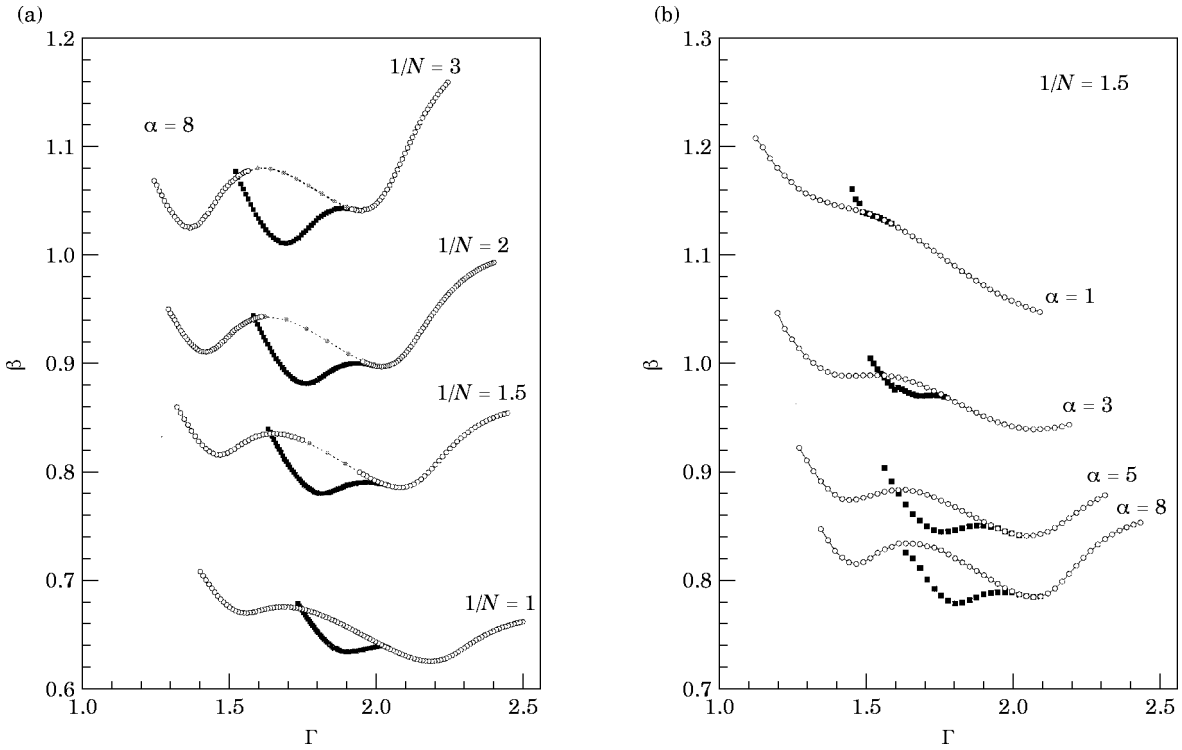

FIG. 12. Selection of the decussate mode versus spiral mode depending on the conicity $1/N$ and the stiffness α. The figures show plots of $\beta = 8\langle G\rangle/N\Gamma^2$ as a function of Γ in the region of competition between the spiral and the decussate modes. Note that β gives the compactness of the cylindrical piling and is only an indicator of the actual compactness in the conical case. This is the reason for the vertical shift of the curves in (a). (a) The four corresponding plots were obtained for the same stiffness $\alpha = 8$ but increasing values of the conicity: from bottom to top $1/N = 1$, 1.5, 2 and 3, respectively. The grey circles indicates regions in which the spiral mode destabilizes spontaneously to the whorled mode in less than 100 particles. The range of stability of the decussate mode as well as its gain in compacity increases with conicity. (b) Three plots corresponding to the same conicity ($1/N = 1.5$) and various values of the stiffness ($\alpha = 1$, 3, 5 and 8). The range of stability of the decussate mode increases with the increase of the interaction stiffness. For the stiffness $\alpha = 1$, the decussate mode is never stable.

4.4. THE ROLE OF THE CONICITY AND OF THE INTERACTION STIFFNESS

The same simulations that we have described in the case of $1/N = 3$ and $\alpha = 8$ were also done for several other values of $1/N$ and α. Although the results were roughly similar, some significant differences appeared.

The steady regimes described above were easily obtained for all values of the stiffness smaller than eight. Stiffer interactions (such as $\alpha = 10$ or 13) do not lead to a good stabilization of the pattern. Very stiff interactions correspond to the packing of hard disks, and in this case any small defect in the arrangement does not vanish with time, but propagates indefinitely (a remark to be found in van Iterson and also Richards, as reported in Snow & Snow, 1962). The use of soft particles in the simulation is the key for the stabilization of the system in perfect patterns.

Within this limit, exploring the dependence of the diagrams $\varphi(\Gamma)$ as a function of $1/N$ and α led to interesting results concerning the selection of the different modes. For instance Figs 10(a) and (b) show the plots of $\varphi(\Gamma)$ and $\varphi(G)$ obtained in the plane situation with circular primordia $1/N = 1$ with $\alpha = 8$. The spiral mode dependence $\varphi(G)$ of Fig. 10(b) is identical to those obtained with imposed periodicity in Part I (Douady & Couder, 1996a) in the case of stiff interaction laws. A comparison of Fig. 10(a) and (b) with Fig. 4(b) and (d) demonstrates the incidence of conicity.

Figures 11(a) and (b) show the evolution of the critical values of Γ and G of the first thresholds as a function of N. They exhibit only a weak dependance on N. This justifies the choice of relation (7) for the definition of Γ and confirms that, as proposed by Snow & Snow (1933), the size of the arc occupied by the new primordium is the dominant factor in the organization. In contrast, the threshold values of G are shifted. A weaker dependence would be found if G/N had been plotted (see relation 12).

The main effect of conicity is that it affects the relative stability of the first whorled and spiral modes. In the plane case $1/N = 1$ (Fig. 10) the opposite

decussate phyllotaxy (2, 2) is missing. By initially imposing elements having the decussate positions we investigated whether or not this mode could keep growing. It was found to do so, but only in a very narrow range of values of Γ.

The exploration of different values of stiffness α show that stiff interactions favour the existence of whorled modes. In contrast, with long range interaction (small α), spiral modes dominate. This can be understood, as the whorled modes present elements that are aligned radially. If the interaction has a long range, the particles placed on the same orthostichy will tend to repel the new ones from this radial line.

These changes in the relative stability of the whorled modes in relation to the spiral ones can be set on a more quantitative basis by a comparison of the plots of their β as a function of Γ. Figure 12(a) shows the relative positions of $\beta(\Gamma)$ of the decussate mode relatively to the values $\beta(\Gamma)$ of the spiral ones for four values of the conicity ($1/N = 1, 1.5, 2, 3$) for a stiffness of $\alpha = 8$. Similarly Fig. 12(b) shows for $1/N = 1$ the effect of increasing stiffness ($\alpha = 3, 5, 8$). A comparison of these curves shows that the effect of increasing conicity or stiffness is to lower the values of β for the decussate mode with respect to the spiral modes. If both $1/N$ and α are large, the decussate mode has a large range of values of Γ for which it is stable as was the case in Fig. 4. Reciprocally, in the plane configuration, the decussate mode has a narrow range of stability and is not observed spontaneously, in agreement with the results shown in Fig. 10. For less stiff interaction it can even cease to exist altogether.

A careful study of the β curves provides an explanation for the selection of the opposite decussate modes with some conicity. In Fig. 8 (obtained with a conicity 1/3) it can be observed that practically all the minima of the different curves lie on the same line. The same property is observed without conicity ($1/N = 1$). This means that all these minima correspond to equally favourable packings and that whorled or spiral patterns are equally good organizations. This is not true, however, for the first transitions. Figure 8 clearly shows that the first minima (1, 1, 2), (1, 2, 3) and (2, 2, 4) are located above the others. This effect is larger on the curve $\beta(\Gamma)$ obtained in the case of $1/N = 1$.

This can be understood by comparison with the cylindrical model quoted above (Douady, 1996). Whenever Γ is very small the model remains reasonably close to the piling of disks on a cylinder. When Γ becomes of the order of unity, however, the effects of the radial characteristic of the conical and plane geometries become dominant. For instance the packing of circular primordia on a plane in an opposite decussate mode cannot be close to the hexagonal ideal. The result is an upward shift of β for the lowest orders (Fig. 8).

4.5. THE ROLE OF THE GROWTH OF THE ELEMENTS SIZE

In all the simulations reported above (except for Fig. 9) we used elements of a constant size. In botanical reality the size of the primordia actually increases with time. This growth of the element's size was taken into account by van Iterson (1907) in his geometrical models. Snow & Snow (1962) insist that the effect of expanding elements would be to stabilize the pattern. As the physiological process of the interaction is not known with certainty, it is not clear whether or not the extension of the inhibiting influence of the primordia grows with the elements' size. In several models using diffusion, the inhibiting activity of the primordia was considered to decrease with time. In any case it is easy to modify our model to introduce elements which generate a potential energy of repulsion which vary as they are advected away from the center. This is realized if, in eqns (1) and (2), the constant size d_0 is replaced by a variable size given by the relation (3). We performed a few series of simulations of this type using the same interactions laws. Patterns obtained with growing primordia were shown in Fig. 9. The corresponding $\varphi(\Gamma)$ diagram is given in Fig. 13: a comparison with Fig. 4 shows that the general

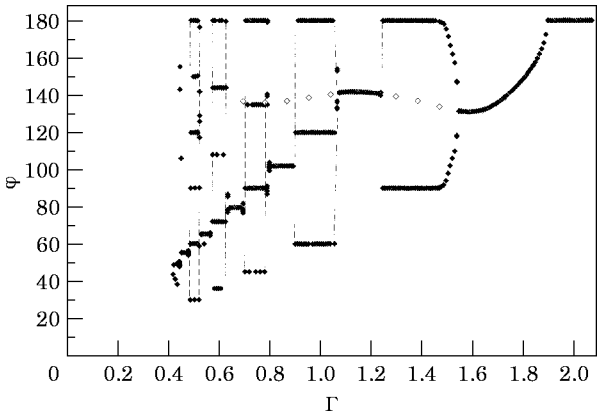

FIG. 13. Diagram of the steady divergence φ as a function of Γ for the patterns obtained with a conicity $1/N = 3$ and a stiffness $\alpha = 8$ in the case where the elements grow in size proportionally to r their distance to the center [eqn (3)]. The black points are stable modes obtained during a very slow decrease of Γ. The open ones correspond to unstable patterns observed transitorily. Comparison with Fig. 4 shows a shift of the thresholds, an increase in the amplitude of the oscillations of the main branch and a larger range of stability of the whorl modes.

aspect of $\varphi(\Gamma)$ is qualitatively unchanged. The thresholds are, however, shifted to smaller values of Γ and the range of stability of the whorled modes is enlarged. Opposite effects are observed if we impose that the size of the primordia decreases with r (corresponding to a hypothetical weakening of their inhibiting potential).

5. PARTIAL CONCLUSION

In the botanical literature there is well-established evidence showing that the formation of the primordia is an iterative process. In these first two articles we sought the minimum hypotheses necessary for this iteration to produce the phyllotactic patterns. Our results, limited here to the steady regimes, show that the very simple rules of the second set of hypotheses are sufficient to produce all the existing structures (except in specific exceptions such as the case of *Costus* discussed in Part I or horse tails to be described in Part III). On the other hand the system did not produce any structure that does not exist in nature.

Our work links several previous results and shows their relation with one another. Investigating dynamical hypotheses from the works of Hofmeister (1868) and Snow & Snow (1952) we found a selection of the patterns directly related to the results obtained by van Iterson (1907) in a purely geometrical approach to phyllotaxy. This shows that the dynamical hypothesis leads to a spontaneous organization into regular patterns, the regular patterns that van Iterson investigated. In doing so, we demonstrated that the dynamics provides a link between van Iterson's parameter Γ and the plastochrone ratio $a=\exp(VT/R_0)$ introduced by Richards (1951). We find that they are related through the packing efficiency β, a parameter which proves essential for the understanding of the selection amongst the various patterns.

Our results are also coherent with previous findings obtained in the analysis of the case of a diffusive interaction. The first simulations showing the spontaneous formation of a Fibonacci order were done by Veen & Lindenmayer (1977), Mitchison (1977), Young (1978) and Meinhardt (1982) in a system controlled by the diffusion of an inhibitor. Veen & Lindenmayer (1977) and Friedman (1992) had also obtained the decussate and trimerous whorled modes together with spiral modes, depending on initial conditions. Their hypotheses were of the Snows' type: any region in which the inhibitor concentration decreases below a threshold becomes a primordium. Mitchison (1977), was the first to give an interpretation for the transition from a Fibonacci mode (i, j) to the next $(i, i+j)$ in the case of a model using a diffusive inhibition on a cylindrical surface. Our results are conceptually in perfect agreement with theirs. Generally, however, our results suggest that the independent physiological decrease of activity used in diffusion models is not necessary to obtain the phyllotactic patterns (even though it might correspond to the physiological reality in the plant).

Owing to their simplicity, we found it useful to present the results of the first model before turning to the second one. Their difference lies in what is imposed and what results. In the first case the periodicity is imposed. If we had examined in Part I the value of the potential in the place where the new particle forms it would certainly have displayed a dependence on G with weak fluctuations, revealing the quality of the piling. In other terms, the new particle was forced to form in the largest available space, but the size of this space had no reason to be constant. In the second case the potential, and thus the size of the available, space is imposed so that the periodicity is a result and it is its average which reflects the density of the piling. The results have shown that the periodicity does not have to be imposed: it appears spontaneously in simulations of the Snows' type. The most stable mode is the one which minimizes the time $\langle T \rangle$ or the packing β. Spatially this means that the system tends to create the structure with the largest density. A comparison of diagrams $\beta(\Gamma)$ for different values of $1/N$ have shown that the role of conicity is to lower the average periodicity β of the decussate mode relatively to that of the spiral ones.

If there is compatibility between the symmetry of several modes, long iterations will always induce a transition towards the stable mode of smallest β. It should be noted, however, that a mode can remain metastable during short transients. This is important, as it suggests that the botanically relevant modes are not always the most stable.

In these first two parts we limited ourselves to the investigation of the idealized models "as such". The reality of the growth of a plant is different from the idealized situation. In the actual growth the number of successive primordia is not very large. The control parameter, either Γ or G, is very generally a decreasing function of time while the conicity $1/N$ usually decreases. In the third part (Douady & Couder, 1996b) we will examine whether or not the models are able to reproduce the real ontogeny of plants. We will see that most botanical transient regimes can be obtained.

REFERENCES

Bravais, L. & Bravais, A. (1837). Essai sur la disposition des feuilles curvisériées. *Ann. Sci. Nat.* **7,** 42–110, Essai sur la disposition symmétrique des inflorescences. 193–221 and 291–348; *Ann. Sci. Nat.* **8,** 11–42.

Bravais, L. & Bravais, A. (1839). Essai sur la disposition des feuilles rectisériées. *Ann. Sci. Nat.* **12,** 5–14 and 65–77.

Couder, Y. & Douady, S. (1993). Phyllotaxis: genetic determination and self organization. In: *Organisation et Processus dans les Systèmes Biologiques*, (Friedel, J. & Gros, F., eds) Technique et Documentation, Paris.

Douady, S. (1996). The packing efficiency of the phyllotaxic patterns on a cylinder. Preprint.

Douady, S. & Couder, Y. (1992). Phyllotaxis as a physical self organised growth process. *Phys. Rev. Lett.* **68,** 2098–2101.

Douady, S. & Couder, Y. (1996a). Phyllotaxis as a self organizing iterative process: part (I) The spiral modes resulting from time periodic iterations. *J. theor. Biol.*, **178,** 255–274.

Douady, S. & Couder, Y. (1996b). Phyllotaxis as a self organizing iterative process: part (III) The simulation of the transient regimes of ontogeny. *J. theor. Biol.*, **178,** 295–312.

Dutrochet, R. J. H. (1834). Observations sur les variations accidentelles du mode suivant lequel les feuilles sont distribuées sur les tiges des végétaux. *Now. Ann. Mus. Hist. Nat.* **3,** 161–200.

Friedman, D. (1992). On whorled/spiral phyllotaxis. In: *Spiral Symmetry* (Hargittai, I. & Pickover, C. A., eds) Singapore: World Scientific.

Green, P. B., Havelange, A. & Bernier, G. (1991). Floral morphogenesis in *Anagallis*: scanning electron micrograph sequences from individual growing meristems before, during and after the transition to flowering. *Planta* **185,** 502–512.

Hernandez, L. F., Havelange, A., Bernier, G. & Green, P. B. (1991). Growth behaviour of single epidermal cells during flower formation: sequential scanning electron micrographs provide kinematic patterns for *Anagallis*. *Planta* **185,** 139–147.

Hofmeister, W. (1868). *Allgemeine Morphologie der Gewâchse*, *Handbuch der Physiologishen Botanik*, 1 Engelmann, Leipzig, 405–664.

Levitov, L. S. (1991*a*) Energetic approach to phyllotaxis. *Europhys. Lett.* **14,** 533–539.

Levitov, L. S. (1991*b*). Phyllotaxis of flux lattices in layered superconductors. *Phys. Rev. Lett.* **66,** 224–227.

Medford, J. I., Behringer, F. J., Callos, J. D. & Feldmann, K. A. (1992). Normal and abnormal development in the *Arabidopsis* vegetative shoot apex. *Plant Cell* **4,** 631–643.

Meicenheimer, R. D. (1979). Changes in *Epilobium* phyllotaxy induced by N-1-naphtylphthalamic acid and α-4-chlorophenoxy-isobutiric acid. *Am. J. Botany* **66,** 557–569.

Meicenheimer, R. D. (1982). Change in *Epilobium* phyllotaxy during the reproductive transition. *Am. J. Botany* **69,** 1108–1118.

Meicenheimer, R. D. & Zagorska-Marek, B. (1989). Consideration of the geometry of the phyllotaxic triangular units and discontinuous phyllotactic transitions. *J. theor. Biol.* **139,** 359–368.

Meinhardt, H. (1982). *Models of Biological Pattern Formation*. London: Academic Press.

Mitchison, G. H. (1977). Phyllotaxis and the Fibonacci series. *Science* **196,** 270–275.

Richards, F. J. (1951). Phyllotaxis: its quantitative expression and relation to growth in the apex. *Phil. Trans. Roy. Soc. B* **225,** 509–564.

Ridley, J. N. (1986). Ideal phyllotaxis on general surfaces of revolution. *Math. Biosciences* **79,** 1–24.

Schoute, J. C. (1913). Beiträge zur Blattstellungslehre. *Rec. Trav. Bot. Néerl.* **10,** 153–339.

Schoute, J. C. (1922). On whorled phyllotaxis (I) growth whorls. *Rec. Trav. Bot. Néerl.* **19,** 184–206.

Schoute, J. C. (1925). On whorled phyllotaxis (II) Late binding whorls of *Peperomia*. *Rec. Trav. Bot. Néerl.* **22,** 128–172.

Schoute, J. C. (1936). On whorled phyllotaxis (III) True and false whorls. *Rec. Trav. Bot. Néerl.* **33,** 670–687.

Schoute, J. C. (1938). On whorled phyllotaxis (IV) Early binding whorls. *Rec. Trav. Bot. Néerl.* **35,** 416–558.

Snow, M. & Snow, R. (1933). Experiments on phyllotaxis, II, the effect of displacing a primordium. *Phil. Trans. Roy. Soc.* **B222,** 353–400.

Snow, M. & Snow, R. (1935). Experiments on phyllotaxis. III. Diagonal splits through decussate apices. *Phil. Trans. Roy. Soc.* **B225,** 63–94.

Snow, M. & Snow, R. (1952). Minimum areas and leaf determination. *Proc. Roy. Soc.* **B139,** 545–566.

Snow, M. & Snow, R. (1962). A theory of the regulation of phyllotaxis based on *Lupinus albus*. *Phil. Trans. Roy. Soc.* **B244,** 483–514.

Turing, A. M. (1952). The chemical basis of morphogenesis. *Phil. Trans. Roy. Soc.* **B237,** 37–72.

van Iterson, G. (1907). *Mathematische und Microscopisch-Anatomische Studien über Blattstellungen*, *nebst Betrachungen über den Schalenbau der Miliolinen*. Iena: Gustav-Fischer-Verlag.

Veen, A. H. & Lindenmayer, A. (1977). Diffusion mechanism for phyllotaxy. *Plant Physiol.* **60,** 127–139.

Wardlaw, C. W. (1968). *Essays on Forms in Plants*. Manchester: Manchester University Press.

Weisse, A. (1894). Neue Beiträge zur mechanischen Blattstellungslehre. *Jahrb. Wiss. Bot.* **26,** 236–294.

Williams, R. F. (1975). *The Shoot Apex and the Leaf Growth*. Cambridge: Cambridge University Press.

Young, D. A. (1978). On the diffusion theory of phyllotaxis. *J. theor. Biol.* **71,** 421–432.

Zagorska-Marek, B. (1987). Phyllotaxis triangular unit: phyllotaxic transitions as the consequences of the apical wedge disclinations in a crystal like pattern of the units. *Acta Soc. Bot. Poloniae* **56,** 229–255.

APPENDIX

Calculation of the Conical Cases in the Plane

The computation of the interaction of elements on a cylinder or on a cone (or equivalently on the plane projection) presents a specific problem. Following van Iterson, the simplest way to understand the cone and its projection is to return to the well-known practical way of its constructing. Taking a plane sheet of paper, simply cut away the paper between two radial lines forming an angle $\Delta\theta$, and join together the two edges. The resulting cone has an angle at the summit $\Psi/2$

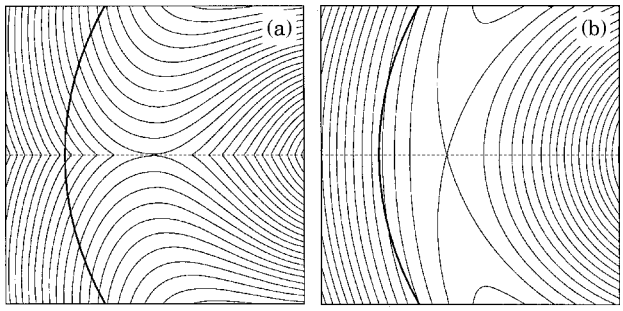

Fig. 14. The equipotential lines created by a single particle located on the other side of the apex. The border of the apex is the arc of circle drawn in bold. (a) If the distance is computed from formula (13) there is a singular line at $\varphi = 180°$. (b) The singularity is smoothed out when relation (6) is used.

which is given by $\sin(\Psi/2) = (2\pi - \Delta\theta)/2\pi$. With this construction, the distance to the centre is preserved while the angles, viewed from above, are increased by a factor $1/\sin(\Psi/2) = 2\pi/(2\pi - \Delta\theta)$. We can thus define the positions of points of the cone by their positions in polar coordinates in the initial plane, the origin being taken at the summit. The distance between these two points is then computed in polar coordinates in the plane. The distance on the cone is obtained if in this distance the angle $(\theta_1 - \theta_0)$ separating the two points is multiplied by the conicity factor $N = \sin(\Psi/2)$:

$$d(P_0, P_1) = \sqrt{(r_0 - r_1)^2 + 2r_0 r_1 (1 - \cos N(\theta_0 - \theta_1)} \tag{A.1}$$

where $(\theta_1 - \theta_0)$ is taken between $-\pi$ and $+\pi$. This formula has the great disadvantage, however, of presenting a discontinuity in its derivative when the second point intersects the line opposite to the first point ($\theta_1 - \theta_0 = \pm\pi$) [cf Fig. 14(a)]. For instance, if the second point moves away from the first point around the cone ($r_1 = r_0$, $\theta_1 - \theta_0$ increasing), the distance increases first linearly, then decreases back when it intersects the opposite direction. If we use the formula $E(d)$ to compute the energy, the energy profile will thus also present a downward cusp along the radial line opposite to the position of the repulsing primordia [Fig. 14(a)]. This discontinuity is problematic, the first reason being that it can induce many artificial effects. For instance, this sharp minimum in the opposite position will evidently strongly favour all patterns such as the distichous mode and the opposite decussate mode where a particle is located in the opposite position [this could have affected the numerical simulation of Friedman (1992)]. The second reason is that it is unrealistic: if we imagine, for instance, that the repulsion is caused by the diffusion of an inhibitor, the resulting profile on the other side of the cylinder will be smooth. The real solution would thus be to compute the final energy profile corresponding to the infinite sum of all the terms $E(d)$ with $2\pi k$ (with k integer) being successively added to $\theta_1 - \theta_0$. For simplicity, we preferred to use the artifice consisting in constructing directly a new "distance" d which does not present this discontinuity, while giving a similar shape [cf Fig. 14(b)]:

$$d(P_0, P_1) = \sqrt{\frac{r_0 - r_1^2}{N} + 2N\, r_0 r_1 (1 - \cos(\theta_0 - \theta_1))} \tag{A.2}$$

The same problem of a discontinuity in the derivative occurs in the extreme case of a cylinder, and it can be solved in the same way. This problem is in fact one of common occurrence in numerical simulation whenever there are boundaries with a periodicity rule. A classical solution is then to replace the parameter presenting the discontinuity, here $\theta_1 - \theta_0$, by its sinus, $\sin(\theta_1 - \theta_0)$. We can also note that this problem arose only because we assumed that the repulsion occurs on the surface only. If we had assumed that the repulsion occurred through the volume, it would not have existed.

It is also worth noting that this discontinuity is only a problem with soft interactions and large values of Γ. The discussion has no meaning if rigid discs are used. In this case, however, a different problem arises: the stabilization of a perfect pattern becomes increasingly difficult because any imperfection of the pattern propagates indefinitely.

Finally, with the definition (6) for the distances, the sustaining angle ω is no longer exactly given by relation (5) but by:

$$\omega = 2\cos^{-1}\left[1 - \frac{1}{N^2}(-1 + \sqrt{1 - N^2\Gamma^2/4})\right] \tag{A.3}$$